THE JOURNAL OF PHYSICAL CHEMISTRY A

pubs.acs.org/JPCA Article

High-Resolution Photoelectron Imaging and Photodetachment Spectroscopy of Cryogenically Cooled IO^-

Yong-Tian Wang, Chuan-Gang Ning, Hong-Tao Liu,* and Lai-Sheng Wang*

Cite This: J. Phys. Chem. A 2020, 124, 5720−5726 Read Online

ACCESS | Metrics & More | Article Recommendations

ABSTRACT: We report a high-resolution photoelectron imaging and photodetachment spectroscopy study of cryogenically cooled IO^-. The high-resolution photoelectron spectra yield a more accurate electron affinity (EA) of 2.3805(5) eV for IO as well as a more accurate spin−orbit splitting energy between the $^2\Pi_{3/2}$ and $^2\Pi_{1/2}$ states of IO as 2093(5) cm^{-1}. Photodetachment spectroscopy confirmed several excited states for the IO^- anion predicted by theoretical calculations, including two valence-type excited states, the repulsive $^3\Pi$ state, and a shallow bound $^1\Pi$ state. More interestingly, we have observed two vibrational resonances which are proposed to be due to a dipole-induced resonant state, about 230 cm^{-1} above the detachment threshold of IO^-.

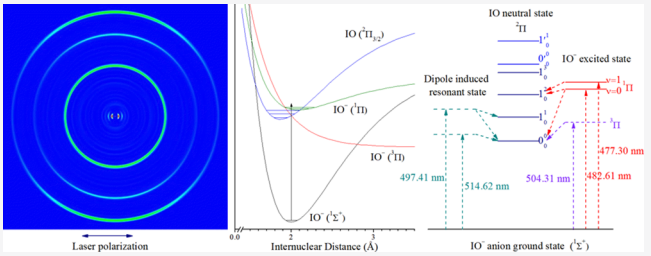

1. INTRODUCTION

It is well-known that halogen species in the atmosphere often exist as catalysts for photochemical reactions related to ozone destruction. For example, the iodine atomic radical reacts with ozone to form IO, which can react with itself or other halogen oxides (BrO or ClO) to form O_2 and halogen atoms. If these species react with ozone, then each catalytic cycle destroys two ozone molecules. The IO radical also reacts with HO_2 to form HOI, which is rapidly photolyzed into I and OH. This catalytic cycle also effectively destroys ozone.[1] Salomon et al. speculated that the catalytic reaction of the IO radical was partly responsible for the lower stratospheric ozone depletion and the sudden disappearance of ozone in the arctic troposphere in the Spring. Recently, iodine monoxide has been observed in space following a volcanic eruption by satellite measurements.[2] Anionic species have recently been directly observed at a high altitude.[3] Studies on the photoexcitation and gas phase reactions of the IO radical and the IO^- anion are essential for understanding atmospheric ion chemistry.[4−8] Photoelectron spectroscopy (PES) of IO^- has been reported by Lineberger and co-workers about 30 years ago.[9,10] The electron affinity (EA), vibrational frequency, and low-lying excited states of IO have been well characterized. However, the photoexcitation and predissociation state of IO^- are not well understood experimentally, although it has been predicted theoretically.[11,12]

Strong spin−orbit (SO) coupling splits the $^2\Pi$ ground state of IO into two SO states ($^2\Pi_{3/2}$, $^2\Pi_{1/2}$), where the $^2\Pi_{1/2}$ state is 2091(40) cm^{-1} higher than the $^2\Pi_{3/2}$ ground state.[9] There are many spectroscopic studies on the strong $A1^2\Pi_{3/2} \leftarrow X1^2\Pi_{3/2}$ electronic transition. The spectrum of $A1^2\Pi_{3/2} \leftarrow X1^2\Pi_{3/2}$ of IO was first observed by Vaidya in the emission spectrum of methyl iodide−methanol.[13] Durie and Ramsay measured the absorption spectrum of IO and determined six vibrational levels. Because the SO splitting in the ground electronic state is very large, no $X2^2\Pi_{1/2}$ state is found in the absorption spectrum.[14] Subsequently, Durie, Legay, and Ramsay observed the A1−X1 system in the emission spectrum and obtained the rotational constant of the ground vibrational level of the X1 state.[15] Bekooy et al. studied the rotational spectra of the 2−0, 2−1, and 2−2 vibrational bands of the $A^2\Pi_{3/2}-X^2\Pi_{3/2}$ system of the IO radicals by molecular beam laser excitation spectroscopy and observed the hyperfine Λ-doublet split of the ground state for the first time.[16] Newman et al. measured the spectral constants and lifetimes of the vibrational energy levels $v' = 0-5$ of the $A^2\Pi_{3/2}$ state of IO using cavity ring-down spectroscopy.[17]

In addition to the spectroscopic studies of the IO $A1^2\Pi_{3/2} \leftarrow X1^2\Pi_{3/2}$ transition, there have been a few detailed spectral studies on the electronic states of $X^2\Pi$ and $A^2\Pi$. Carrington et al. and Brown et al. used electron resonance spectra to study IO $X^2\Pi$ and determined the approximate spin−orbit splitting.[18,19] Tamassia et al. studied the overtone band of IO X2(2−0) by laser magnetic resonance and determined the vibration, rotation, spin−orbit, λ-doubling, hyperfine, and Zeeman parameters.[20] Miller et al. explored the rotational

Received: May 7, 2020
Revised: June 15, 2020
Published: June 29, 2020

https://dx.doi.org/10.1021/acs.jpca.0c04080
J. Phys. Chem. A 2020, 124, 5720−5726

spectra of the ground state and the two lowest vibrational levels of the IO $X^2\Pi_{3/2}$ state.[21] The $A^2\Pi_{3/2}$ state of IO is highly predissociative as the excited state potential energy curve is crossed by a repulsive electronic potential energy curve that results in dissociation of the I−O bond.[22] The study of the A-state shows that the predissociation from $v' = 1, 4, 5$ is very fast and the lifetime of $v' = 2$ depends on the rotational level, while the predissociation from the $v' = 0, 3$ levels is independent of rotation.[4]

Molecules with sufficiently large dipole moments can bind electrons in a diffuse orbital to form weakly bound negative ions,[23−25] which can have excited dipole bound states (DBSs) just below the detachment threshold. DBSs in excited anions were first observed as resonances in photodetachment cross sections[26,27] and were studied by rotational autodetachment spectroscopy.[28−34] Recently, photodetachment spectroscopy of cryogenically cooled anions has allowed DBSs to be observed in many valence-bound anions,[35−39] enabling the development of resonant photoelectron spectroscopy via vibrational autodetachment.[40] Theoretical and experimental studies have shown that the empirical minimum dipole moment to support a DBS in molecular systems is 2.5 D.[41−43] Recently, electronically excited DBSs for a series of halogen-substituted phenoxide anions, p-$XC_6H_4O^-$ (X = F, Cl, Br, I), have been observed by Qian et al., who found that the binding energies of the DBSs exhibit a linear correlation with the dipole moments of the neutral cores and confirmed that the critical dipole moment for the existence of DBSs is 2.5 D.[44] The dipole moment of IO is determined to be 2.45 D by studying the Stark splitting in gas phase electron resonance spectroscopy,[45] which is slightly below the threshold value. It would be interesting to know if a DBS exists below the detachment threshold of the IO^- anion.

Previous PES experiments[9,10] showed that the SO splitting of IO [2091(40) cm^{-1}] is significantly larger than the IO vibrational frequency (681 cm^{-1}).[9,16] The vibrational frequency of the neutral IO is known to be much larger than that for the anion [581(25) cm^{-1}], consistent with the fact that photodetachment comes from an antibonding orbital. Vibrational quanta only up to 2 for IO^- were observed in the previous PES experiments with the EA for IO being determined to be 2.378(6) eV. Excited states with predissociative character for the IO^- anion have been predicted[12] but have not been observed experimentally.

In the current work, we have obtained a more accurate EA and spin−orbit splitting energy using high-resolution PE imaging of cryogenically cooled IO^- anions. Photodetachment spectroscopy was carried out, resulting in the observation of several excited states of IO^-. A resonantly enhanced vibrational peak of $v = 2$ and a new vibrational peak ($v = 3$) were observed for the first time for the ground state detachment transition. The possible photoabsorption to a predissociation state of IO^- has been observed. More interestingly, we have observed a DBS-like excited for IO^-, which we call a "dipole-induced resonant state".

2. EXPERIMENTAL METHODS

The current experiments were performed by using the third-generation ESI-PES apparatus,[46] equipped with an electrospray ionization (ESI) source,[47] a cryogenically controlled ion trap,[48] and a high-resolution PE imaging system.[49,50] Electrospray of an NaI solution mixed with water and ethanol was used to prepare the IO^- anions, in which IO^- could be steadily produced by tuning the ESI conditions. The anions from the ESI source were delivered to a temperature-controlled ion trap,[48] where they were accumulated and cooled for about 0.1 s before being injected into a time-of-flight mass spectrometer. The IO^- anions were selected by a mass gate and then focused into a collinear velocity-map imaging lens,[50] where anions were photodetached by a linearly polarized laser beam. The photodetachment laser was from a dye laser system (Sirah, line width 0.03 cm^{-1} at 500 nm) pumped by a Nd:YAG laser. The output wavelength was calibrated with a Bristol 821 wavelength meter. Photoelectrons were projected onto a detector consisting of a pair of microchannel plates and a phosphor screen. The photoelectron images were captured by a charge-coupled-device (CCD) camera, and the 3D electron velocity distribution is reconstructed by using the BASEX program.[51] The PE spectra were obtained by integrating the signals from the respective images radially. The electron kinetic energy was proportional to the square of the radius (r^2) and was calibrated by the known spectra of Au^-. The binding energy spectra were obtained by subtracting the kinetic energy spectrum from the respective detachment photon energies. The imaging system could achieve an electron energy resolution of ∼2 cm^{-1} for low-energy electrons in this study.[49]

The advantage of photoelectron imaging is that it enables simultaneous measurement of the photoelectron angular distribution (PAD) for each detachment transition, which reflects the symmetry of the parent anion orbital.[52] The differential cross section of the angular distribution is given by[53,54]

$$\frac{d\sigma}{d\Omega} = \frac{\sigma_{tot}}{4\pi}[1 + \beta P_2(\cos\theta)] \quad (1)$$

where σ_{tot} is the total detachment cross section, $P_2(x)$ is the second-order Legendre polynomial, θ is the angle of the outgoing electron's velocity vector with respect to the laser polarization direction, and β is the anisotropy parameter, ranging from −1 to 2 for purely perpendicular and parallel transitions, respectively.

3. RESULTS AND DISCUSSION

3.A. High-Resolution Photoelectron Imaging. The PE images and spectra of IO^- are shown in Figure 1 at five photon energies. Highly resolved vibrational features of the ground state ($^2\Pi_{3/2}$) were obtained in the low photon energy spectra, as shown in Figure 1a to 1c, and the excited state ($^2\Pi_{1/2}$) was also observed at the higher photon energies in Figure 1d and 1e. In the current work, we use 0_0^0 to represent the transition from the ground vibrational level of the ground electronic state of $IO^-(^1\Sigma^+)$ to that of the neutral states of IO($^2\Pi$) and 1_0^n (n = 1−3) to indicate transitions to the vibrational excited states of the neutral states. The vibrational features of the $^2\Pi_{1/2}$ state are labeled with an apostrophe to distinguish them from those of the $^2\Pi_{3/2}$ state. The current work extends the previous studies[9,10] and yields more accurate spectroscopic constants. First, the cryogenically cooled ions completely eliminated vibrational hot bands and resulted in much better resolved spectra. The 0 ← 0 transition (0_0^0) of the $^2\Pi_{3/2}$ state in Figure 1a defines a highly accurate EA of 2.3805 ± 0.0005 eV for IO compared to 2.378 ± 0.005 eV reported previously.[9,10] The vibrational frequencies for the two spin−orbit states was measured to be 682(5) cm^{-1} for the $^2\Pi_{3/2}$ state and 639(5) cm^{-1} for the $^2\Pi_{1/2}$ state, consistent with 681.6 cm^{-1} for $^2\Pi_{3/2}$ state and 658(25) for the $^2\Pi_{1/2}$ state reported previously.[9,10,16]

https://dx.doi.org/10.1021/acs.jpca.0c04080
J. Phys. Chem. A 2020, 124, 5720−5726

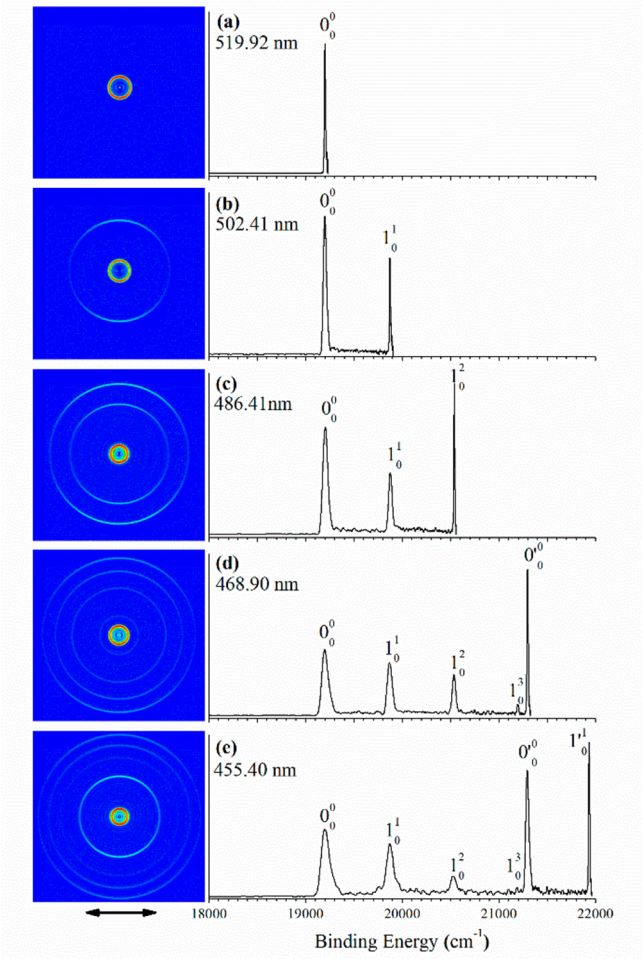

Figure 1. Photoelectron images and spectra of IO^- at (a) 519.92, (b) 502.41, (c) 486.41, (d) 468.90, and (e) 455.40 nm. The observed vibrational structures are labeled and the excited state vibrational peaks are labeled with an apostrophe. The photon energies were chosen to be near each vibrational transition. The double arrow below the images indicates the laser polarization.

In addition, we observed a weak vibrational peak (ν = 3) (Figure 1d) that was not observed previously due to the high spectral resolution and the elimination of the vibrational hot bands in the current experiment. Finally, the anisotropic parameters (β) for all vibrational peaks at the different kinetic energies were obtained, as summarized in Table 1. The angular distributions suggest a s+d wave for the outgoing electron, consistent with detachment from a π-orbital.

We also observed a significant threshold enhancement effect for the ν = 2 vibration peak (Figure 1c). A more accurate spin−orbit splitting energy of 2093(5) cm^{-1} was obtained for the IO ground state between $^2\Pi_{3/2}$ and $^2\Pi_{1/2}$. Spectroscopic constants for the two spin−orbit states of IO are summarized in Table 2. The dissociation energy (D_0) of IO^- to give I^- and O can be derived to be 1.708 eV by using the following thermodynamic relation:

$$D_0(I{-}O^-) = EA(IO) - EA(I) + D_0(I{-}O)$$

or 3.306(9) eV to give I and O^- by using the following relationship:

$$D_0(I{-}O^-) = EA(IO) - EA(O) + D_0(I{-}O)$$

where EA for the IO is from the current experiment, the EAs for the I and O are 3.0590 and 1.4611 eV, respectively,[55] and the I−O dissociation energy is 54.9(0.2) kcal/mol (2.387 eV).[56]

Table 2. Spectroscopic Constants for Both Spin−Orbit States of Neutral IO

state	r_e (Å)	ω_e (cm^{-1})	$\omega_e\chi_e$ (cm^{-1})	energy (cm^{-1})	EA (eV)
IO $a^2\Pi_{1/2}$	1.887(10)[9]	639(5)	4.37[16]	2093(5)	2.3805(5)
IO $X^2\Pi_{3/2}$	1.8676[16]	682(5)	4.50	0	

3.B. Resonant Photoelectron Imaging and Photodetachment Spectroscopy. At certain detachment wavelengths, the angular distribution of the PE images and the peak intensities are significantly different, as shown in Figure 2; five resonant images and spectra are obtained at five different photon energies. When we tuned the detachment laser to 514.62 nm (Figure 2a), we observed only the 0_0^0 transition, whereas at 497.41 nm (Figure 2c), we observed both the 0_0^0 and the 1_0^1 transitions. However, the PE images appeared more isotropic, different from the distinct s+d angular distributions shown in Figure 1. According to the data given in Table 1, the anisotropy parameters at these two wavelengths were still negative but closer to zero for a complete isotropic distribution. These observations indicated that the electron signals were likely from autodetachment from resonantly excited states of the IO^- anion.

Table 1. Anisotropic Parameters (β) Values for All Vibrational Peaks at the Different Kinetic Energies

		vibrational peaks				
	photo energy (nm)	0_0^0	1_0^1	1_0^2	$0'^0_0$	$1'^1_0$
Figure 1a	519.92	−0.24(01)				
Figure 1b	502.41	−0.64(02)	−0.32(01)			
Figure 1c	486.41	−0.83(02)	−0.72(03)	−0.33(01)		
Figure 1d	468.90	−0.76(04)	−0.55(06)	−0.18(17)[a]	−0.50(01)	
Figure 1e	455.40	−0.78(08)	−0.36(14)[a]	−0.15(30)[a]	−0.48(04)	−0.39(05)
Figure 2a	514.62	−0.14(01)				
Figure 2b	504.31	−0.18(01)				
Figure 2c	497.41	−0.35(01)	−0.24(01)			
Figure 2d	482.61	−0.30(04)	−0.57(16)[a]	−0.19(02)		
Figure 2e	477.30	−0.64(06)	−0.57(10)	−0.20(06)		

[a]The uncertainties of these values are relatively large because the signal of their corresponding vibrational peaks is weak.

https://dx.doi.org/10.1021/acs.jpca.0c04080
J. Phys. Chem. A 2020, 124, 5720−5726

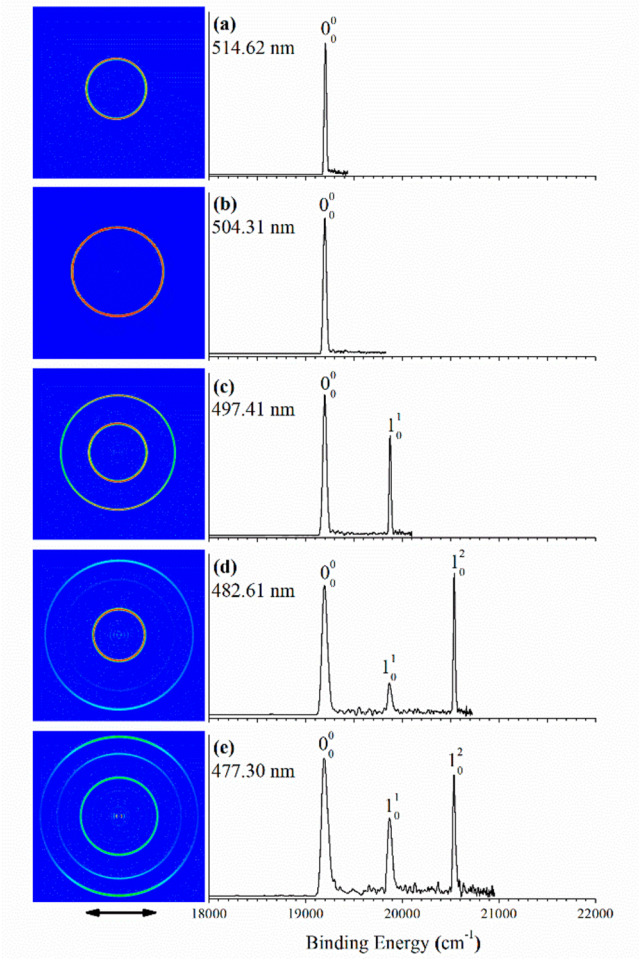

Figure 2. Resonant photoelectron images and spectra of IO^- at (a) 514.62, (b) 504.31, (d) 497.41, (d) 482.61, and (e) 477.30 nm. The wavelengths were determined from the photodetachment spectrum (see Figure 3). The double arrow below the images indicates laser polarization.

We scanned our detachment laser near 514 and 497 nm by monitoring the electron signal of the 0_0^0 transition to obtain a photodetachment spectrum. We indeed observed two resonant peaks, as shown in Figure 3. The centers of these two peaks are located at 514.62 and 497.41 nm, respectively. As shown in Figures 2a and 2c, the PE images at these two wavelengths should come from both direct detachment from the ground state of the IO^- anion and autodetachment from the excited state of IO^-. The interval between these two resonant peaks is 672 cm^{-1}, which is identical with the vibrational frequency (673 cm^{-1}) of the neutral IO in its ground state. Therefore, these resonances appeared to be from two vibrational levels of a DBS because it is known that the DBS electron has little effect on the structure of the neutral core.[34,57,58] However, when we tuned the photon energy below the detachment threshold (2.3085 eV) for scanning, we did not find any resonance signals. Hence, there is a possibility that we have observed a dipole-induced state, but it is not bound, similar to a Feshbach resonance.[59,60] In the current case, the dipole-induced Feshbach resonance is 230 cm^{-1} above the detachment threshold of IO^-.

In addition, we also observed several other resonances in the photodetachment spectrum in Figure 3. The peak shape of the resonance at 504.31 nm was intense and did not seem to be

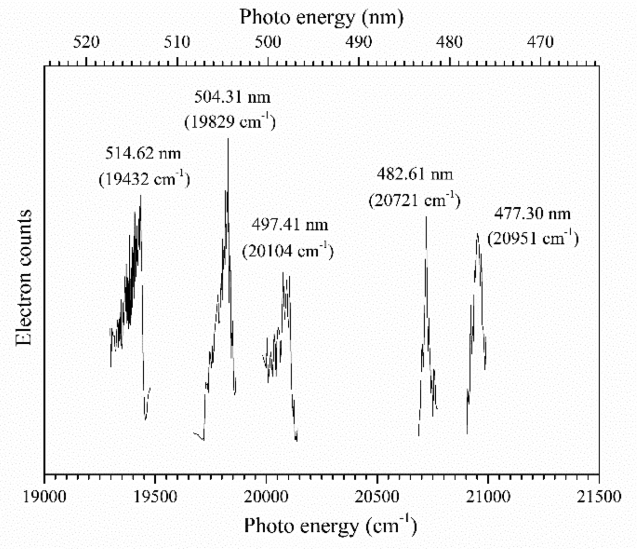

Figure 3. Photodetachment spectrum of IO^- obtained by measuring the total electron yield as a function of photo energy.

related to the "dipole induced resonance" mentioned above. We suspected that this resonance was due to the predissociative Π state of the IO^- molecular anion. A previous theoretical calculation by Minaev et al.[12] showed that the IO^- anion is stable in the ground $X^1\Sigma^+$ state which dissociates to the excited state $I^-(^1S)$ + $O(^1D)$ limit; the lowest excited $^3\Pi$ state is repulsive, and its dissociation limit is $I^-(^1S)$ + $O(^3P)$, which is lower in energy by 2 eV than the dissociation limit of $X^1\Sigma^+$ state. The crossing of the vibrational level of the $X^1\Sigma^+$ state with the repulsive $a^3\Pi$ state causes predissociation. The resonance at 504.31 nm was very likely due to excitation to the $a^3\Pi$ state. The resonant PE spectrum at 504.31 nm (Figure 2b) also gave a nearly isotropic angular distribution.

The two peaks at 482.61 and 477.30 nm with an interval of 230 cm^{-1} on the right in Figure 3 were narrower than the three peaks on the left. These two resonant peaks with narrower line widths should be due to a single vibrational progression of an electronically excited state of IO^-. The peak at 482.61 nm is assigned as the vibrational ground state because we did not observe any more vibrational peaks with an interval close to 230 cm^{-1} when the laser was scanned to lower photo energies. Thus, the vibrational ground level of this excited state of IO^- is 1521 cm^{-1} above the detachment threshold of IO^-, and the fundamental vibrational frequency for the IO^- excited state is determined to be 230 ± 5 cm^{-1}. When we tuned the detachment laser to 482.61 nm (Figure 2d), the resonant PE spectra showed the $\nu = 2$ peak was significantly enhanced. The photoelectron angular distributions of both the $\nu = 0$ and $\nu = 2$ peaks were more isotropic ($\beta = -0.30$ and -0.19; see Table 1), which are very different from the $\nu = 1$ peak ($\beta = -0.57$). The resonant PE spectra measured at 477.30 nm (Figure 2e) showed that only the $\nu = 2$ peak was significantly enhanced and its angular distribution was more isotropic ($\beta = -0.20$). These observations are quite different in comparison with autodetachment from DBS vibrational levels, which obeys the $\Delta\nu = -1$ propensity rule.

Calculations by Minaev et al. predicted two low-lying excited Π states for the IO^- anion.[12] The $^3\Pi$ state of IO^- was repulsive, and its crossing with the $X^2\Pi_{3/2}$ state of IO causes predissociation, which is assigned to the resonance at 504.31

https://dx.doi.org/10.1021/acs.jpca.0c04080
J. Phys. Chem. A 2020, 124, 5720−5726

nm as discussed above. We assign the two resonances at the higher excitation energies to the $^1\Pi$ excited state of IO^-. The peak widths for these two resonances were measured to be about 40 cm^{-1}, from which we estimated a lifetime of ~0.13 ps for the observed excited states of IO^-. Hence, the $^1\Pi$ excited state should be a bound state with a shallow potential well (230 cm^{-1} frequency), in contrast to the predicted repulsive state.[12] Figure 4 displays the schematic potential energy curves

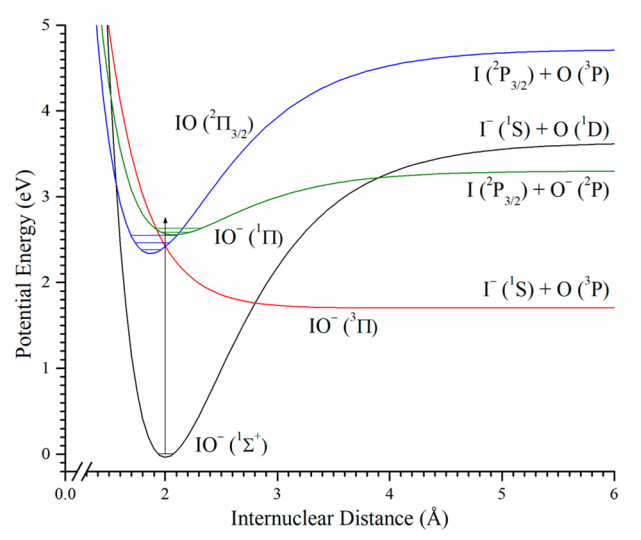

Figure 4. Schematic potential curves of the neutral IO and of the IO^- anion. The potential energy curves were estimated based on the state assignments.

of IO and IO^- according to the current experimental observations. In light of the current results, more accurate theoretical calculation for the excited states of IO^- seems warranted, including the nature of the dipole-dominated excited state.

4. CONCLUSION

In summary, we have obtained a more accurate electron affinity for IO as 2.3805(5) eV and a more accurate spin−orbital splitting energy between the $^2\Pi_{3/2}$ and $^2\Pi_{1/2}$ states as 2093(5) cm^{-1} by using high-resolution photoelectron imaging of cold IO^-. Photodetachment spectroscopy revealed several resonances for IO^-. A theoretically predicted excited state ($^3\Pi$) with predissociative character and an excited state ($^1\Pi$) of IO^- anion were found to be 20,721 cm^{-1} (2.5690 ± 0.0005 eV) above the ground state of IO^- and 1521 cm^{-1} (0.1886 ± 0.0005 eV) above the detachment threshold of IO^-. Two additional resonances were observed and were proposed to be from a dipole-induced Feshbach resonance.

AUTHOR INFORMATION

Corresponding Authors

Hong-Tao Liu − *Key Laboratory of Interfacial Physics and Technology, Shanghai Institute of Applied Physics, Chinese Academy of Sciences, Shanghai 201800, P. R. China;* orcid.org/0000-0001-6450-2585; Email: liuhongtao@sinap.ac.cn

Lai-Sheng Wang − *Department of Chemistry, Brown University, Providence, Rhode Island 02912, United States;* orcid.org/0000-0003-1816-5738; Email: lai-sheng_wang@brown.edu

Authors

Yong-Tian Wang − *Key Laboratory of Interfacial Physics and Technology, Shanghai Institute of Applied Physics, Chinese Academy of Sciences, Shanghai 201800, P. R. China; University of Chinese Academy of Sciences, Beijing 100049, P. R. China*

Chuan-Gang Ning − *Department of Physics, State Key Laboratory of Low-Dimensional Quantum Physics, Tsinghua University, Beijing 100084, P. R. China*

Complete contact information is available at: https://pubs.acs.org/10.1021/acs.jpca.0c04080

Notes

The authors declare no competing financial interest.

ACKNOWLEDGMENTS

The experimental work (done at Brown) was supported by the U.S. Department of Energy, Office of Basic Energy Sciences, Chemical Science, Geosciences, and Bioscience Division under Grant DE-SC0018679 (to L.S.W.). The work done in Shanghai was supported by the National Natural Science Foundation of China (21573273 and 21773289). H.-T.L. also acknowledges Supported by the "Transformational Technologies for Clean Energy and Demonstration", Strategic Priority Research Program of the Chinese Academy of Sciences (Grant XDA21000000), and the K.C. Wong Education Foundation (Grant GJTD-2018-10).

REFERENCES

(1) Alicke, B.; Hebestreit, K.; Stutz, J.; Platt, U. Iodine oxide in the marine boundary layer. *Nature* **1999**, *397* (6720), 572.

(2) Schönhardt, A.; Richter, A.; Theys, N.; Burrows, J. P. Space-based observation of volcanic iodine monoxide. *Atmos. Chem. Phys.* **2017**, *17* (7), 4857−4870.

(3) Frege, C.; Bianchi, F.; Molteni, U.; Tröstl, J.; Junninen, H.; Henne, S.; Sipilä, M.; Herrmann, E.; Rossi, M. J.; Kulmala, M.; et al. Chemical characterization of atmospheric ions at the high altitude research station Jungfraujoch (Switzerland). *Atmos. Chem. Phys.* **2017**, *17* (4), 2613−2629.

(4) Roszak, S.; Krauss, M.; Alekseyev, A.; Liebermann, H.-P.; Buenker, R. Spin− Orbit Configuration Interaction Calculation of the Potential Energy Curves of Iodine Oxide. *J. Phys. Chem. A* **2000**, *104* (13), 2999−3003.

(5) Saiz-Lopez, A.; Plane, J. M.; Baker, A. R.; Carpenter, L. J.; von Glasow, R.; Martin, J. C.; McFiggans, G.; Saunders, R. W. Atmospheric chemistry of iodine. *Chem. Rev.* **2012**, *112* (3), 1773−1804.

(6) Teiwes, R.; Elm, J.; Handrup, K.; Jensen, E. P.; Bilde, M.; Pedersen, H. B. Atmospheric chemistry of iodine anions: elementary reactions of I^-, IO^-, and IO_2^- with ozone studied in the gas-phase at 300 K using an ion trap. *Phys. Chem. Chem. Phys.* **2018**, *20* (45), 28606−28615.

(7) Dillon, T. J.; Blitz, M. A.; Heard, D. E. Determination of the rate coefficients for the reactions IO + NO_2 + M (air) –> $IONO_2$ + M and O(3P) + NO_2 –> O_2 + NO using laser-induced fluorescence spectroscopy. *J. Phys. Chem. A* **2006**, *110* (21), 6995−7002.

(8) Gomez Martin, J. C.; Galvez, O.; Baeza-Romero, M. T.; Ingham, T.; Plane, J. M.; Blitz, M. A. On the mechanism of iodine oxide particle formation. *Phys. Chem. Chem. Phys.* **2013**, *15* (37), 15612−15622.

(9) Gilles, M. K.; Polak, M. L.; Lineberger, W. Photoelectron spectroscopy of IO^-. *J. Chem. Phys.* **1991**, *95* (6), 4723−4724.

(10) Gilles, M. K.; Polak, M. L.; Lineberger, W. Photoelectron spectroscopy of the halogen oxide anions FO^-, ClO^-, BrO^-, IO^-, $OClO^-$, and OIO^-. *J. Chem. Phys.* **1992**, *96* (11), 8012−8020.

https://dx.doi.org/10.1021/acs.jpca.0c04080
J. Phys. Chem. A 2020, 124, 5720−5726

(11) Lee, L. C.; Smith, G. P.; Moseley, J. T.; Cosby, P. C.; Guest, J. A. Photodissociation and photodetachment of Cl_2^-, ClO^-, Cl_3^- and $BrCl_2^-$. *J. Chem. Phys.* **1979**, *70* (7), 3237−3246.
(12) Minaev, B.; Loboda, O.; Vahtras, O.; Ågren, H.; Bilan, E. Physical properties and spectra of IO, IO^- and HOI studied by ab initio methods. *Spectrochim. Acta, Part A* **2002**, *58* (5), 1039−1053.
(13) Vaidya, W. In *The Flame Spectra of Some Aliphatic Halides—Part I*; Proceedings of the Indian Academy of Sciences, Section A; Springer: 1937; pp 122−128.
(14) Durie, R. A.; Ramsay, D. Absorption spectra of the halogen monoxides. *Can. J. Phys.* **1958**, *36* (1), 35−53.
(15) Durie, R.; Legay, F.; Ramsay, D. An emission system of the IO molecule. *Can. J. Phys.* **1960**, *38* (3), 444−452.
(16) Bekooy, J.; Meerts, W. L.; Dymanus, A. High-resolution laser-rf spectroscopy on the $A^2\Pi_{3/2}$-$X^2\Pi_{3/2}$ system of iodine oxide (IO). *J. Mol. Spectrosc.* **1983**, *102* (2), 320−343.
(17) Newman, S. M.; Howie, W. H.; Lane, I. C.; Upson, M. R.; Orr-Ewing, A. J. Predissociation of the $A^2\Pi_{3/2}$ state of IO studied by cavity ring-down spectroscopy. *J. Chem. Soc., Faraday Trans.* **1998**, *94* (18), 2681−2688.
(18) Carrington, A.; Dyer, P. N.; Levy, D. H. Gas-Phase Electron Resonance Spectra of BrO and IO. *J. Chem. Phys.* **1970**, *52* (1), 309−314.
(19) Brown, J. M.; Byfleet, C. R.; Howard, B. J.; Russell, D. K. The electron resonance spectra of BrO, IO and SeF in J = 5/2 rotational levels. *Mol. Phys.* **1972**, *23* (3), 457−468.
(20) Tamassia, F.; Kermode, S. M.; Brown, J. M. A Study of the (2−0) Overtone Bands of the FO, BrO, and IO Free Radicals by Laser Magnetic Resonance. *J. Mol. Spectrosc.* **2001**, *205* (1), 92−101.
(21) Miller, C. E.; Cohen, E. A. Rotational spectroscopy of IO $X\,^2\Pi_i$. *J. Chem. Phys.* **2001**, *115* (14), 6459−6470.
(22) Gravestock, T. J.; Blitz, M. A.; Heard, D. E. A laser induced fluorescence study relating to physical properties of the iodine monoxide radical. *Phys. Chem. Chem. Phys.* **2010**, *12* (4), 823−834.
(23) Fermi, E.; Teller, E. The Capture of Negative Mesotrons in Matter. *Phys. Rev.* **1947**, *72* (5), 399−408.
(24) Crawford, O. H. Negative ions of polar molecules. *Mol. Phys.* **1971**, *20* (4), 585−591.
(25) Garrett, W. Critical binding of an electron to a non-stationary electric dipole. *Chem. Phys. Lett.* **1970**, *5* (7), 393−397.
(26) Zimmerman, A. H.; Brauman, J. I. Resonances in electron photodetachment cross sections. *J. Chem. Phys.* **1977**, *66* (12), 5823−5825.
(27) Jackson, R. L.; Hiberty, P. C.; Brauman, J. I. Threshold resonances in the electron photodetachment spectrum of acetaldehyde enolate anion. Evidence for a low-lying, dipole-supported state. *J. Chem. Phys.* **1981**, *74* (7), 3705−3712.
(28) Wetzel, D. M.; Brauman, J. I. Rotational structure in an excited vibronic band of the dipole-supported state of cyanomethyl anion, CH_2CN^-. *J. Chem. Phys.* **1989**, *90* (1), 68−73.
(29) Lykke, K. R.; Mead, R. D.; Lineberger, W. C. Observation of Dipole-Bound States of Negative Ions. *Phys. Rev. Lett.* **1984**, *52* (25), 2221−2224.
(30) Lykke, K. R.; Neumark, D. M.; Andersen, T.; Trapa, V. J.; Lineberger, W. C. Autodetachment spectroscopy and dynamics of CH_2CN^- and CD_2CN^-. *J. Chem. Phys.* **1987**, *87* (12), 6842−6853.
(31) Yokoyama, K.; Leach, G. W.; Kim, J. B.; Lineberger, W. C.; Boldyrev, A. I.; Gutowski, M. Autodetachment spectroscopy and dynamics of vibrationally excited dipole-bound states of H_2CCC^-. *J. Chem. Phys.* **1996**, *105* (24), 10706−10718.
(32) Pino, T.; Tulej, M.; Güthe, F.; Pachkov, M.; Maier, J. P. Photodetachment spectroscopy of the $C_{2n}H^-$ (n = 2−4) anions in the vicinity of their electron detachment threshold. *J. Chem. Phys.* **2002**, *116* (14), 6126−6131.
(33) Jagau, T. C.; Dao, D. B.; Holtgrewe, N. S.; Krylov, A. I.; Mabbs, R. Same but Different: Dipole-Stabilized Shape Resonances in CuF^- and AgF^-. *J. Phys. Chem. Lett.* **2015**, *6* (14), 2786−2793.
(34) Czekner, J.; Cheung, L. F.; Kocheril, G. S.; Wang, L. S. Probing the coupling of a dipole-bound electron with a molecular core. *Chem. Sci.* **2019**, *10* (5), 1386−1391.
(35) Liu, H. T.; Ning, C. G.; Huang, D. L.; Dau, P. D.; Wang, L. S. Observation of mode-specific vibrational autodetachment from dipole-bound states of cold anions. *Angew. Chem., Int. Ed.* **2013**, *52* (34), 8976−8979.
(36) Huang, D. L.; Liu, H. T.; Ning, C. G.; Wang, L. S. Vibrational state-selective autodetachment photoelectron spectroscopy from dipole-bound states of cold 2-hydroxyphenoxide: o-$HO(C_6H_4)O^-$. *J. Chem. Phys.* **2015**, *142* (12), 124309.
(37) Huang, D. L.; Liu, H. T.; Ning, C. G.; Wang, L. S. Conformation-Selective Resonant Photoelectron Spectroscopy via Dipole-Bound States of Cold Anions. *J. Phys. Chem. Lett.* **2015**, *6* (12), 2153−2157.
(38) Huang, D. L.; Zhu, G. Z.; Wang, L. S. Communication: Observation of dipole-bound state and high-resolution photoelectron imaging of cold acetate anions. *J. Chem. Phys.* **2015**, *142* (9), 091103.
(39) Zhu, G. Z.; Qian, C. H.; Wang, L. S. Tautomer-Specific Resonant Photoelectron Imaging of Deprotonated Cytosine Anions. *Angew. Chem., Int. Ed.* **2019**, *58* (23), 7856−7860.
(40) Zhu, G. Z.; Wang, L. S. High-resolution photoelectron imaging and resonant photoelectron spectroscopy via noncovalently bound excited states of cryogenically cooled anions. *Chem. Sci.* **2019**, *10* (41), 9409−9423.
(41) Turner, J. E. Minimum dipole moment required to bind an electron—molecular theorists rediscover phenomenon mentioned in Fermi-Teller paper twenty years earlier. *Am. J. Phys.* **1977**, *45* (8), 758−766.
(42) Jordan, K. D.; Wang, F. Theory of dipole-bound anions. *Annu. Rev. Phys. Chem.* **2003**, *54*, 367−396.
(43) Simons, J. Molecular anions. *J. Phys. Chem. A* **2008**, *112* (29), 6401−6511.
(44) Qian, C. H.; Zhu, G. Z.; Wang, L. S. Probing the Critical Dipole Moment To Support Excited Dipole-Bound States in Valence-Bound Anions. *J. Phys. Chem. Lett.* **2019**, *10* (21), 6472−6477.
(45) Byfleet, C.; Carrington, A.; Russell, D. Electric dipole moments of open-shell diatomic molecules. *Mol. Phys.* **1971**, *20* (2), 271−277.
(46) Wang, L.-S. Perspective: Electrospray photoelectron spectroscopy: From multiply-charged anions to ultracold anions. *J. Chem. Phys.* **2015**, *143* (4), 040901.
(47) Wang, L.-S.; Ding, C.-F.; Wang, X.-B.; Barlow, S. E. Photodetachment photoelectron spectroscopy of multiply charged anions using electrospray ionization. *Rev. Sci. Instrum.* **1999**, *70* (4), 1957−1966.
(48) Wang, X. B.; Wang, L. S. Development of a low-temperature photoelectron spectroscopy instrument using an electrospray ion source and a cryogenically controlled ion trap. *Rev. Sci. Instrum.* **2008**, *79* (7), 073108.
(49) Leon, I.; Yang, Z.; Wang, L. S. High resolution photoelectron imaging of Au_2^-. *J. Chem. Phys.* **2013**, *138* (18), 184304.
(50) Leon, I.; Yang, Z.; Liu, H. T.; Wang, L. S. The design and construction of a high-resolution velocity-map imaging apparatus for photoelectron spectroscopy studies of size-selected clusters. *Rev. Sci. Instrum.* **2014**, *85* (8), 083106.
(51) Dribinski, V.; Ossadtchi, A.; Mandelshtam, V. A.; Reisler, H. Reconstruction of Abel-transformable images: The Gaussian basis-set expansion Abel transform method. *Rev. Sci. Instrum.* **2002**, *73* (7), 2634−2642.
(52) Sanov, A. Laboratory-frame photoelectron angular distributions in anion photodetachment: insight into electronic structure and intermolecular interactions. *Annu. Rev. Phys. Chem.* **2014**, *65*, 341−363.
(53) Cooper, J.; Zare, R. N. Angular distribution of photoelectrons. *J. Chem. Phys.* **1968**, *48* (2), 942−943.
(54) Cooper, J.; Zare, R. N. Erratum: Angular distribution of photoelectrons. *J. Chem. Phys.* **1968**, *49*, 4252.

https://dx.doi.org/10.1021/acs.jpca.0c04080
J. Phys. Chem. A 2020, 124, 5720−5726

(55) Peláez, R. J.; Blondel, C.; Delsart, C.; Drag, C. Pulsed photodetachment microscopy and the electron affinity of iodine. *J. Phys. B: At., Mol. Opt. Phys.* **2009**, *42* (12), 125001.
(56) Dooley, K. S.; Geidosch, J. N.; North, S. W. Ion imaging study of IO radical photodissociation: Accurate bond dissociation energy determination. *Chem. Phys. Lett.* **2008**, *457* (4−6), 303−306.
(57) Liu, H. T.; Ning, C. G.; Huang, D. L.; Wang, L. S. Vibrational spectroscopy of the dehydrogenated uracil radical by autodetachment of dipole-bound excited states of cold anions. *Angew. Chem., Int. Ed.* **2014**, *53* (9), 2464−2468.
(58) Huang, D.-L.; Liu, H.-T.; Ning, C.-G.; Dau, P. D.; Wang, L.-S. Resonant photoelectron imaging of deprotonated uracil anion via vibrational levels of a dipole-bound excited state. *Chem. Phys.* **2017**, *482*, 374−383.
(59) Chin, C.; Grimm, R.; Julienne, P.; Tiesinga, E. Feshbach resonances in ultracold gases. *Rev. Mod. Phys.* **2010**, *82* (2), 1225.
(60) Leon, I.; Yang, Z.; Wang, L. S. Resonant photoelectron spectroscopy of Au_2^- via a Feshbach state using high-resolution photoelectron imaging. *J. Chem. Phys.* **2013**, *139* (19), 194306.

https://dx.doi.org/10.1021/acs.jpca.0c04080
J. Phys. Chem. A 2020, 124, 5720−5726